

Modeling of axion and electromagnetic fields coupling in a particle-in-cell code

Xiangyan An,^{1,2,3} Min Chen,^{1,2, a)} Jianglai Liu,³ Zhengming Sheng,^{1,2,3} and Jie Zhang^{1,2,3}

¹⁾Key Laboratory for Laser Plasmas (MoE), School of Physics and Astronomy, Shanghai Jiao Tong University, Shanghai 200240, China

²⁾Collaborative Innovation Center of IFSA, Shanghai Jiao Tong University, Shanghai 200240, China

³⁾Tsung-Dao Lee Institute, Shanghai Jiao Tong University, Shanghai 200240, China

(Dated: June 25, 2024)

Axions have aroused widespread research interest because they can solve the strong CP problem and serve as a possible candidate for dark matter. Currently, people have explored a lot of axion detection experiments, including passively detecting the existing axions in the universe, and actively generating axions in the laboratory. Recently, axion-coupled laser-plasma interactions have been discussed as a novel method to detect axions. Petawatt (PW) lasers are considered as a powerful tool to study not only the vacuum polarization but also the axion coupling, due to their extreme fields. However, particle-in-cell (PIC) simulation is still missed in current studies, which limits the understanding of axion-coupled laser-plasma interactions. In this paper, we proposed the method to include the axion field and the coupling with electromagnetic (EM) fields in PIC codes. The axion wave equation and modified Maxwell's equations are numerically solved, while the EM field modulation from axions is considered as a first-order perturbation. Meanwhile, different axion field boundary conditions are considered to satisfy different simulation scenarios. The processes of conversions between axions and photons, and weak laser pulse propagation with axion effects are checked as benchmarks of the code. Such an extended PIC code may help researchers develop novel axion detection schemes based on laser-plasma interactions and provide a better understanding of axion-coupled astrophysical processes.

I. INTRODUCTION

Axion was initially proposed by Wilczek¹ and Weinberg² as the resulted particle from spontaneously broken of Peccei-Quinn (PQ) symmetry^{3,4}, to solve the strong CP problem⁵. Besides, axions are also considered as one of the possible candidates for dark matter^{5,6}.

Currently, there are many axion detection experiments around the world. One way is to detect the existing axions, including those from the sun and universe background. In this scenario, there are Axion Dark Matter Experiment (ADMX)⁷⁻⁹ to convert dark matter axions into microwave photons and CERN Axion Solar Telescope (CAST)¹⁰ to convert solar axions into X-ray photons in magnetic fields to detect axions. Besides, people are also seeking axion hints in some astrophysical phenomena¹¹⁻¹³.

Besides passively detecting the existing axions in the universe, some groups also actively generate axions and detect the derivative effects. Polarization rotation of a laser in a transverse magnetic field is thought to be a signal of axion existence, such as PVLAS¹⁴, BMV¹⁵, BFRT¹⁶, and Q&A¹⁷ experiments. Meanwhile, there is also an effective laser experiment named "light shining through a wall". A laser is used to generate axions through a magnetic region, after which a wall is used to block the laser photon and only the axions can transmit

the wall. Then the axions will be reconverted into photons in a second magnetic region to be detected. Such a scheme is used in ALPS¹⁸, GammeV¹⁹, LIPSS²⁰, OSQAR²¹, and BMV²².

Although there are currently many detection and experimental setups to search axions and other dark matters in the world, no convincing signals have been discovered so far²³. One possible reason is the weak coupling between axions and photons, $g_{a\gamma\gamma} \lesssim 10^{-10} \text{ GeV}^{-1}$. Meanwhile, high-power lasers are recently considered to enhance the vacuum birefringence (VB) signal²⁴⁻²⁶, which is also the aim of PVLAS, BMV, BFRT and Q&A experiments. Instead of polarization rotation from axion coupling, an initially linear-polarized laser may gain a small ellipticity after propagating through the magnetic field. Such an ellipticity signal can be significantly enhanced with a 10 PW laser (with magnetic fields reaching 10^6 T). Similarly, the polarization rotation signal may also be enhanced through PW lasers.

Moreover, when the laser intensity increases, there could be more new axion-related phenomena to study and detect in laser-plasma interactions. People have found a new quasiparticle from axions coupling to the electrostatic (Langmuir) modes²⁷. Some plasma-based axion generation and detection schemes have also been proposed and discussed²⁸⁻³⁰.

However, current studies about axion-coupled laser-plasma interactions are still limited to theoretical calculations. To get a comprehensive understanding of the interaction process, PIC is a quite powerful tool. In a PIC code, particle motion is calculated according to

^{a)}Electronic mail: minchen@sjtu.edu.cn

the Lorentz force with modifications from some QED processes, and EM fields are numerically solved according to Maxwell's equations and the current contributed by the particles. Such a method has been successfully used in studying laser wakefield acceleration^{31–34}, strong field quantum electrodynamics (QED) effects^{35,36}, and so on. Despite that, the axion field and the coupling with EM fields are still missed in current usually used PIC codes, which limited the studies about axion-coupled laser-plasma interactions.

In this paper, we added the axion field and the coupling with EM fields into the PIC code EPOCH³⁷. The axion wave equation and modified Maxwell's equations are numerically solved. Since the axion coupling is extremely small, the axion modulation to EM fields is considered a first-order perturbation. Meanwhile, different kinds of axion field boundary conditions are considered to satisfy different simulation scenarios. With such modifications, the code can simulate axion fields self-consistently. In the end, the axion generation from photons and conversion into photons in a constant magnetic field are shown as benchmarks of the code.

II. SIMULATION METHODS

A. Units and Field Equations

In natural units ($\hbar = \varepsilon_0 = c = 1$), the axion coupling with EM fields can be described by the Lagrangian density term $\mathcal{L}_{\text{int}} = -\frac{1}{4}g_{a\gamma\gamma}\phi F_{\mu\nu}G^{\mu\nu} = g_{a\gamma\gamma}\phi \mathbf{E} \cdot \mathbf{B}$, where $g_{a\gamma\gamma}$ is the coupling constant, $F^{\mu\nu}$ and $G^{\mu\nu}$ are the electromagnetic tensor and dual tensor, respectively, and \mathbf{E} , \mathbf{B} are the electric field and magnetic field, respectively. The total Lagrangian density reads,

$$\mathcal{L} = \mathcal{L}_{\text{EM}} + \mathcal{L}_{\phi} + \mathcal{L}_{\text{int}}, \quad (1)$$

$$\mathcal{L}_{\text{EM}} = -\frac{1}{4}F_{\mu\nu}F^{\mu\nu} + A_{\mu}j_e^{\mu}, \quad (2)$$

$$\mathcal{L}_{\phi} = \frac{1}{2}\partial_{\mu}\phi\partial^{\mu}\phi - \frac{1}{2}m_a^2\phi^2, \quad (3)$$

where m_a is the axion mass, \mathcal{L}_{EM} and \mathcal{L}_{ϕ} are the Lagrangian density of EM field and free axion field, respectively. After variation to the total Lagrangian density, we can get the modified Maxwell equations with axion coupling,

$$\partial_t^2\phi - \nabla^2\phi + m_a^2\phi = g_{a\gamma\gamma} \mathbf{E} \cdot \mathbf{B}, \quad (4)$$

$$\nabla \cdot \mathbf{E} = \rho - g_{a\gamma\gamma} \mathbf{B} \cdot \nabla\phi, \quad (5)$$

$$\nabla \cdot \mathbf{B} = 0, \quad (6)$$

$$\nabla \times \mathbf{E} = -\partial_t \mathbf{B}, \quad (7)$$

$$\nabla \times \mathbf{B} = \partial_t \mathbf{E} + \mathbf{j} + g_{a\gamma\gamma}[(\partial_t\phi)\mathbf{B} - \mathbf{E} \times \nabla\phi], \quad (8)$$

where ρ and \mathbf{j} are the electrical charge density and current density, respectively. Here we did not introduce an additional duality symmetry as some other works^{27,28,38}.

The code EPOCH is an open source PIC code and it's widely used in laser plasma community^{37,39–41}. EPOCH makes calculations in SI units. And in SI units, we choose the axion field ϕ to have dimensions of frequency, and the axion coupling constant $g_{a\gamma\gamma}$ to have dimensions of time. In this way, the modified Maxwell equations in SI units read,

$$\left(\frac{\partial^2}{c^2\partial t^2} - \nabla^2 + \frac{m_a^2 c^2}{\hbar^2}\right)\phi = \frac{g_{a\gamma\gamma}}{\hbar\mu_0} \mathbf{E} \cdot \mathbf{B}, \quad (9)$$

$$\nabla \cdot \mathbf{E} = \frac{\rho}{\varepsilon_0} - cg_{a\gamma\gamma} \mathbf{B} \cdot \nabla\phi, \quad (10)$$

$$\nabla \cdot \mathbf{B} = 0, \quad (11)$$

$$\nabla \times \mathbf{E} = -\partial_t \mathbf{B}, \quad (12)$$

$$\nabla \times \mathbf{B} = \frac{\partial}{c^2\partial t} \mathbf{E} + \mu_0 \mathbf{j} + \frac{g_{a\gamma\gamma}}{c} [(\partial_t\phi)\mathbf{B} - \mathbf{E} \times \nabla\phi]. \quad (13)$$

B. Perturbations due to Axion Field

First of all, we need to notice that the axion modulation to the EM fields might be so small that it would be overwhelmed by the floating point error. To solve this problem, we use field perturbation separation (FPS) method by expanding the variables according to the order of axion coupling: $\mathbf{E} = \mathbf{E}_0 + \mathbf{E}_1$, $\mathbf{B} = \mathbf{B}_0 + \mathbf{B}_1$, $\rho = \rho_0 + \rho_1$, $\mathbf{j} = \mathbf{j}_0 + \mathbf{j}_1$, where \mathbf{E}_0 , \mathbf{B}_0 , ρ_0 , \mathbf{j}_0 satisfy the Maxwell equations without axion. Then the first-order perturbations of the EM fields satisfy,

$$\nabla \cdot \mathbf{E}_1 = \frac{\rho_1}{\varepsilon_0} - cg_{a\gamma\gamma} \mathbf{B}_0 \cdot \nabla\phi, \quad (14)$$

$$\nabla \cdot \mathbf{B}_1 = 0, \quad (15)$$

$$\nabla \times \mathbf{E}_1 = -\partial_t \mathbf{B}_1, \quad (16)$$

$$\nabla \times \mathbf{B}_1 = \frac{\partial}{c^2\partial t} \mathbf{E}_1 + \mu_0 \mathbf{j}_1 + \frac{g_{a\gamma\gamma}}{c} [(\partial_t\phi)\mathbf{B}_0 - \mathbf{E}_0 \times \nabla\phi]. \quad (17)$$

As an estimation, for a laser with the normalized vector potential $a_0 = |eE_0/(m_e\omega_0c)| = 100$ (where $\omega_0 = ck_0 = 2\pi c/\lambda_0$ is the laser frequency, and e , m_e are the electron charge and mass, respectively), the non-perturbed electric field is $E_0 = 4 \times 10^{14}$ V/m for an 800 nm laser. Considering such a laser generating axions in a magnetic field as strong as itself within a wavelength, the generated axion field is approximately $\frac{g_{a\gamma\gamma}E_0B_0}{2\mu_0\hbar k_0^2} = 5.7 \times 10^9 \text{ s}^{-1}$ (for a typical $g_{a\gamma\gamma} = 2.7 \times 10^{-13} \hbar \text{ GeV}^{-1}$). With such an axion field, the axion modulation to the EM field can be estimated as $E_1 \approx g_{a\gamma\gamma}\phi B_0 c = 4 \times 10^{-13}$ V/m.

Unfortunately, the value of E_0 is represented as a double precision floating-point number in the program. In binary, such a number is $E_0 \stackrel{\text{bin}}{=} 1.\underbrace{011\dots0}_{52} \times 2^{48}$ V/m. To

represent such a number, the computer would use 1 bit for the \pm sign, 11 bits for the exponent, and 52 bits for the mantissa. Therefore, the minimal step for E_0 to increase

is error (E_0) = $2^{-52} \times 2^{48} = 0.0625$ V/m, which is called the floating point error of E_0 . We can see that E_1 is even far less than the floating point error: $E_1 \ll \text{error}(E_0)$. Therefore, it is necessary to treat the zero and first order EM fields independently according to Eq. 14-17. Otherwise, E_1 would be overwhelmed by the floating point error of E_0 and we can never get the correct modulation from the axion fields.

Moreover, since Eq. 14 can be derived from Eq. 17 and the continuity equation $\partial_t \rho_1 + \nabla \cdot \mathbf{j}_1 = 0$ together, we only need to treat the current perturbation \mathbf{j}_1 in the code. For this part, we consider the perturbation to the particle momentum and velocity: $\mathbf{p} = \mathbf{p}_0 + \mathbf{p}_1$, $\mathbf{v} = \mathbf{v}_0 + \mathbf{v}_1$. To calculate the perturbed particle motion, we should first calculate the perturbed fields felt by the particle, which are given by ($F = E_{x,y,z}$, $B_{x,y,z}$ is the example field component):

$$\begin{aligned}
F|_{\mathbf{x}=\mathbf{x}_0+\mathbf{x}_1} &= (F_0 + F_1)|_{\mathbf{x}=\mathbf{x}_0+\mathbf{x}_1} \\
&= \sum_{ijk} S(\mathbf{r}_{ijk} - \mathbf{x}_0 - \mathbf{x}_1) (F_{0,ijk} + F_{1,ijk}) \\
&\approx \sum_{ijk} S(\mathbf{r}_{ijk} - \mathbf{x}_0) F_{0,ijk} \\
&+ \sum_{ijk} \left[\frac{\partial S(\mathbf{r}_{ijk} - \mathbf{x})}{\partial \mathbf{x}} \Big|_{\mathbf{x}=\mathbf{x}_0} \cdot \mathbf{x}_1 \right] F_{0,ijk} \\
&+ \sum_{ijk} S(\mathbf{r}_{ijk} - \mathbf{x}_0) F_{1,ijk} \\
&= F_{\text{nop}} + F_{\text{p}},
\end{aligned} \tag{18}$$

where $S(\mathbf{r}_{ijk} - \mathbf{x})$ is the shape function of a particle locating at position \mathbf{x} , \mathbf{r}_{ijk} is the space grid position of the corresponding field component, $F_{\text{nop}} = \sum_{ijk} S(\mathbf{r}_{ijk} - \mathbf{x}_0) F_{0,ijk}$ and F_{p} are the non-perturbed and perturbed fields felt by the particle. The the perturbed position and momentum of the particle can be calculated according to:

$$\frac{d\mathbf{x}_1}{dt} = \mathbf{v}_1, \tag{19}$$

$$\frac{d\mathbf{p}_1}{dt} = q(\mathbf{E}_{\text{p}} + \mathbf{v}_0 \times \mathbf{B}_{\text{p}} + \mathbf{v}_1 \times \mathbf{B}_{\text{nop}}), \tag{20}$$

$$\mathbf{v}_1 = \frac{\partial \mathbf{v}}{\partial \mathbf{p}} \cdot \mathbf{p}_1 = \frac{c}{\gamma_0^3} [\gamma_0^2 \mathbf{u}_1 - \mathbf{u}_0 (\mathbf{u}_0 \cdot \mathbf{u}_1)], \tag{21}$$

where q and m are the charge and mass of the particle, respectively, and $\mathbf{u} = \mathbf{p}/(mc)$ is the normalized momentum. Then the current perturbation can be calculated

according to the particle shape function:

$$\begin{aligned}
(\mathbf{j}_0 + \mathbf{j}_1)_{ijk} &= \frac{q}{\Delta V} [S(\mathbf{r}_{ijk} - \mathbf{x}_0 - \mathbf{x}_1) (\mathbf{v}_0 + \mathbf{v}_1)] \\
&\approx \frac{q}{\Delta V} S(\mathbf{r}_{ijk} - \mathbf{x}_0) \mathbf{v}_0 \\
&+ \frac{q}{\Delta V} \left[\frac{\partial S(\mathbf{r}_{ijk} - \mathbf{x})}{\partial \mathbf{x}} \Big|_{\mathbf{x}=\mathbf{x}_0} \cdot \mathbf{x}_1 \right] \mathbf{v}_0 \\
&+ \frac{q}{\Delta V} S(\mathbf{r}_{ijk} - \mathbf{x}_0) \mathbf{v}_1,
\end{aligned} \tag{22}$$

where ΔV is the macroparticle volume in the code. So far we have given the full description of the perturbed EM fields in the code, which is necessary to correctly calculate the derivative effects of axions.

C. Field Equations Discretization

In the following, we give the description of axion discretization in both time and space grids. The superscription will label the index of time steps, and the subscription will label the space index. It should be pointed out that a single 0 or 1 on the subscript is used to label the order of the EM field. Although we use SI units in the code, the following equations used in the numerical model will still be shown in natural units for convenience. From the equations, we naturally set the axion fields at the half-time grids. Then the time differential is realized as,

$$\partial_t \phi \rightarrow (D_t \phi)^n = \frac{\phi^{n+\frac{1}{2}} - \phi^{n-\frac{1}{2}}}{\Delta t}, \tag{23}$$

$$\partial_t^2 \phi \rightarrow (D_t^2 \phi)^{n+\frac{1}{2}} = \frac{\phi^{n+\frac{3}{2}} - 2\phi^{n+\frac{1}{2}} + \phi^{n-\frac{1}{2}}}{(\Delta t)^2}, \tag{24}$$

where Δt is the time step. In one time step of the code, we would first update the EM fields for half time step and then update the axion field,

$$\begin{aligned}
\mathbf{E}_1^{n+\frac{1}{2}} &= \mathbf{E}_1^n + \frac{\Delta t}{2} (\nabla \times \mathbf{B}_1^n - \mathbf{j}_1^n \\
&- g_{a\gamma\gamma} [(D_t \phi)^n \mathbf{B}_0^n - \mathbf{E}_0^n \times \nabla \phi^n]),
\end{aligned} \tag{25}$$

$$\mathbf{B}_1^{n+\frac{1}{2}} = \mathbf{B}_1^n - \frac{\Delta t}{2} \nabla \times \mathbf{E}_1^{n+\frac{1}{2}}, \tag{26}$$

$$\frac{\phi^{n+\frac{3}{2}} - 2\phi^{n+\frac{1}{2}} + \phi^{n-\frac{1}{2}}}{(\Delta t)^2} = (\nabla^2 \phi - m_a^2 \phi + g_{a\gamma\gamma} \mathbf{E}_0 \cdot \mathbf{B}_0)^{n+\frac{1}{2}}. \tag{27}$$

The particles are then pushed by both zero and first order fields. After that, we update the EM fields for the left half time step.

$$\mathbf{B}_1^{n+1} = \mathbf{B}_1^{n+\frac{1}{2}} - \frac{\Delta t}{2} \nabla \times \mathbf{E}_1^{n+\frac{1}{2}}, \tag{28}$$

$$\begin{aligned}
\mathbf{E}_1^{n+1} &= \mathbf{E}_1^{n+\frac{1}{2}} + \frac{\Delta t}{2} (\nabla \times \mathbf{B}_1^{n+1} - \mathbf{j}_1^{n+1} \\
&- g_{a\gamma\gamma} [(D_t \phi)^{n+\frac{1}{2}} \mathbf{B}_0^{n+1} - \mathbf{E}_0^{n+1} \times \nabla \phi^{n+1}]).
\end{aligned} \tag{29}$$

Here ϕ^n would be given by the averaged axion fields at two time steps,

$$\phi^n = \frac{1}{2} \left(\phi^{n+\frac{1}{2}} + \phi^{n-\frac{1}{2}} \right). \quad (30)$$

As for the spatial discretization, the configuration is shown in Fig. 1. While the components of EM fields are staggered to the grid boundaries in certain directions, we consider the axion field to locate at the cell center in all directions. In this way, we can calculate the space dependent terms in Eq. 25 and 27.

$$i' = i + \frac{1}{2}, \quad j' = j + \frac{1}{2}, \quad k' = k + \frac{1}{2}, \quad (31)$$

$$\partial_x^2 \phi \rightarrow (D_x^2 \phi)_{i'j'k'} = \frac{\phi^{(i'+1)j'k'} - 2\phi^{i'j'k'} + \phi^{(i'-1)j'k'}}{(\Delta x)^2}. \quad (32)$$

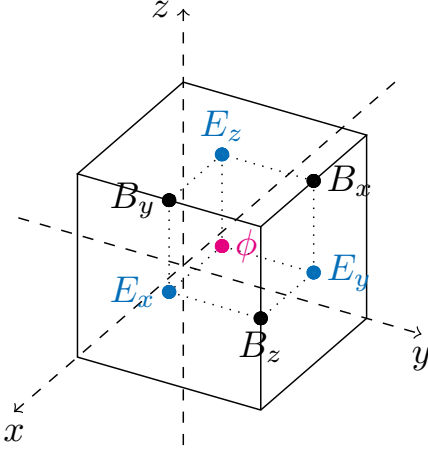


Figure 1. The configuration of EM fields and axion field in the PIC code.

Moreover, to update the axion fields as Eq. 27, we need to calculate the source term $\mathbf{E}_0 \cdot \mathbf{B}_0$ at axion field locations. The actual values of the EM fields are given by averaging the fields at the nearest cells,

$$(\mathbf{E}_0 \cdot \mathbf{B}_0)_{i'j'k'} = \bar{E}_{0x} \bar{B}_{0x} + \bar{E}_{0y} \bar{B}_{0y} + \bar{E}_{0z} \bar{B}_{0z}, \quad (33)$$

$$\bar{E}_{0x} = \frac{1}{2} \left[E_{0x, (i'+\frac{1}{2})j'k'} + E_{0x, (i'-\frac{1}{2})j'k'} \right], \quad (34)$$

$$\begin{aligned} \bar{B}_{0x} = \frac{1}{4} & \left[B_{0x, i'(j'+\frac{1}{2})(k'+\frac{1}{2})} + B_{0x, i'(j'+\frac{1}{2})(k'-\frac{1}{2})} \right. \\ & \left. + B_{0x, i'(j'-\frac{1}{2})(k'+\frac{1}{2})} + B_{0x, i'(j'-\frac{1}{2})(k'-\frac{1}{2})} \right]. \end{aligned} \quad (35)$$

And the other components are averaged similarly. The cross term $\mathbf{E}_0 \times \nabla \phi$ in Eq. 25 is also given by averaging. Here we show the expression of one component

$(\mathbf{E}_0 \times \nabla \phi)_x$, the other components are similar.

$$(\mathbf{E}_0 \times \nabla \phi)_x \rightarrow (E_{0y} D_z \phi - E_{0z} D_y \phi)_{(i'+\frac{1}{2})j'k'}, \quad (36)$$

$$\begin{aligned} (E_{0y} D_z \phi)_{(i'+\frac{1}{2})j'k'} = \frac{1}{4} & \left[E_{0y, i'(j'+\frac{1}{2})k'} + E_{0y, i'(j'-\frac{1}{2})k'} \right] \\ & \cdot \frac{\phi_{i'j'(k'+1)} - \phi_{i'j'(k'-1)}}{2\Delta z} \\ & + \frac{1}{4} \left[E_{0y, (i'+1)(j'+\frac{1}{2})k'} + E_{0y, (i'+1)(j'-\frac{1}{2})k'} \right] \\ & \cdot \frac{\phi_{(i'+1)j'(k'+1)} - \phi_{(i'+1)j'(k'-1)}}{2\Delta z}. \end{aligned} \quad (37)$$

D. Axion Field Boundary Conditions

The solutions of partial differential equations are only complete with specific boundary conditions. As for the boundary conditions of axions, we implemented four kinds of boundary conditions in the code: reflect, periodic, outflow, and PML (Perfectly Matched Layers). These are quite similar as EM field treatments in usual PIC codes, which are used for different scenarios⁴²⁻⁴⁴.

1. Reflect. As for the reflect boundary condition, we set the axion field gradient to zero at the boundary.

$$\phi_{(-\frac{1}{2})j'k'} = \phi_{(\frac{1}{2})j'k'}, \quad \dots \quad (38)$$

2. Periodic. As for the periodic boundary condition, we would set the axion field at the out cell to be the same on the other side.

$$\phi_{(-\frac{1}{2})j'k'} = \phi_{(N_x - \frac{1}{2})j'k'}, \quad \dots, \quad (39)$$

where N_x is the total grid number in x direction.

3. Outflow. As for the outflow boundary condition, we would assume a left-handed wave propagating along x direction at the x_{\min} boundary, or a right-handed wave at the x_{\max} boundary. And the treatments in the y and z directions are similar. Specifically, we solve the two equations at the boundary to obtain the axion fields $\phi_{(-\frac{1}{2})j'k'}^n$ and $\phi_{(-\frac{3}{2})j'k'}^{n-1}$ out of the simulation box at each time step, which are needed to update the axion field in the box. The results are (with the source term $S = g_{a\gamma\gamma} \mathbf{E}_0 \cdot \mathbf{B}_0$),

$$\left[\frac{\Delta t}{\Delta x} + \frac{(\Delta t)^2}{(\Delta x)^2} \right] \phi_{(-\frac{3}{2})j'k'}^{n-1} = -2\phi_{(-\frac{1}{2})j'k'}^{n-1} + 2\phi_{(-\frac{1}{2})j'k'}^{n-2} - (\Delta t)^2 \left[S_{(-\frac{1}{2})j'k'}^{n-1} - m_a^2 \phi_{(-\frac{1}{2})j'k'}^{n-1} \right] + \frac{\Delta t}{\Delta x} \phi_{(\frac{1}{2})j'k'}^{n-1} - \frac{(\Delta t)^2}{(\Delta x)^2} \left[\phi_{(\frac{1}{2})j'k'}^{n-1} - 2\phi_{(-\frac{1}{2})j'k'}^{n-1} \right], \quad (40)$$

$$\phi_{(-\frac{1}{2})j'k'}^n = \phi_{(-\frac{1}{2})j'k'}^{n-2} + \frac{\Delta t}{\Delta x} \left[\phi_{(\frac{1}{2})j'k'}^{n-1} - \phi_{(-\frac{3}{2})j'k'}^{n-1} \right]. \quad (41)$$

4. PML. As for the outflow boundary condition, we would assume the axion field to exponentially decay in the absorbing layer,

$$\phi = \phi_i e^{i(\omega t - kx) - \sigma t}, \quad (42)$$

where σ is an artificial absorbing constant. Thus we made the transform $\partial_t \rightarrow \partial_t + \sigma$ in Eq. 4. Then after discretization, the evolution equation for the axion field in the absorbing layer is,

$$(1 + \sigma \Delta t) \phi_{i'j'k'}^{n+1} = (\Delta t)^2 \left[S_{i'j'k'}^n - m^2 \phi_{i'j'k'}^n \right] + (D_x^2 + D_y^2 + D_z^2) \phi_{i'j'k'}^n - \sigma^2 \phi_{i'j'k'}^n + \sigma \Delta t \phi_{i'j'k'}^{n-1} + 2\phi_{i'j'k'}^n - \phi_{i'j'k'}^{n-1}. \quad (43)$$

III. CODE BENCHMARK

After implementing the axion field and the coupling with EM fields in the code, we can self-consistently simulate the axion generation, propagation, and conversion to EM fields. We first check the different kinds of boundary conditions in the code.

A. Boundary Condition Checking

To check the boundary conditions we used in the code, we would assume a left-handed axion wave $\phi = e^{-(\eta^2 + y^2)/w^2} \sin k_0 \eta$ in the simulation box, where $\eta = x + ct$ is the moving coordinate, $w = 5\lambda_0$ is the duration and width of the test axion pulse, and $\lambda_0 = 2\pi/k_0 = 800 \text{ nm}$ is the axion wavelength. To realize such an axion wave, what we actually do is to set the axion fields $\phi|_{t=\frac{1}{2}\Delta t}$ and $\phi|_{t=-\frac{1}{2}\Delta t}$ at two time steps. In this case, we considered the axion mass as 1 meV, which is much less than the mass cooresponding to the axion wavelength set in the simulation. Since here we only check the axion boundary conditions, the coupling constant $g_{a\gamma\gamma}$ does not matter. Moreover, the simulation box is set to be $[-20\lambda_0, 20\lambda_0] \times [-20\lambda_0, 20\lambda_0]$, and the grid number is 400×400 . As for the PML boundary condition, we set the layer thickness to be $N_{\text{PML}} = 20$ grids in all directions. The maximal absorbing constant is $\sigma_{\text{max}} dt = 0.2$

and the absorbing constant grows in the absorbing layer as $\sigma = \left(1 - \frac{i_{\text{PML}}}{N_{\text{PML}}}\right)^3 \sigma_{\text{max}}$, where i_{PML} is the grid index from the boundary.

Figure 2 shows the results of different boundary conditions. We can see that the axion field can be correctly reflected or propagating to another side with the corresponding reflect or periodic boundary conditions. With outflow or PML boundary conditions, the axion field can transmit out of the boundary or be absorbed by the boundary layer with negligible reflectivity. The numerical reflectivities are both $\sim 1\%$ with the last two boundary conditions.

B. Benchmark of Axion Generation

Moreover, we can further simulate the process of photon-axion and axion-photon conversions in a constant magnetic field. Since the axion wave equation contains the source term $g_{a\gamma\gamma} \mathbf{E} \cdot \mathbf{B}$, a laser propagating in a constant magnetic field parallel to its polarization would continuously generate axions, and vice versa. The conversion probabilities are^{19,45},

$$P_{\gamma \rightarrow \phi} = P_{\phi \rightarrow \gamma} \approx \frac{1}{4} (g_{a\gamma\gamma} B_0 l)^2 \left[\frac{\sin(\kappa l/2)}{\kappa l/2} \right]^2, \quad (\text{natural units}) \quad (44)$$

$$P_{\gamma \rightarrow \phi} = P_{\phi \rightarrow \gamma} \approx \frac{c}{4\mu_0 \hbar} (g_{a\gamma\gamma} B_0 l)^2 \left[\frac{\sin(\kappa l/2)}{\kappa l/2} \right]^2, \quad (\text{SI units}) \quad (45)$$

where $\kappa = k_1 - k_0$ reflects the momentum difference between the photon and axion, k_0, k_1 are the wave vectors of photon and axion, respectively, and l is the laser propagating distance inside the magnetic field.

To simulate the process of axion generation, we consider a p -polarized laser with the wavelength $\lambda_0 = 800 \text{ nm}$ propagating in a magnetic field of $\mathbf{B} = B_c \hat{\mathbf{y}}$. The laser normalized vector potential is $a_0 = |eE/(m_e \omega_0 c)| = 3$ and it carries Gaussian envelopes in both transverse and longitudinal directions. The width is $5\lambda_0$ and the

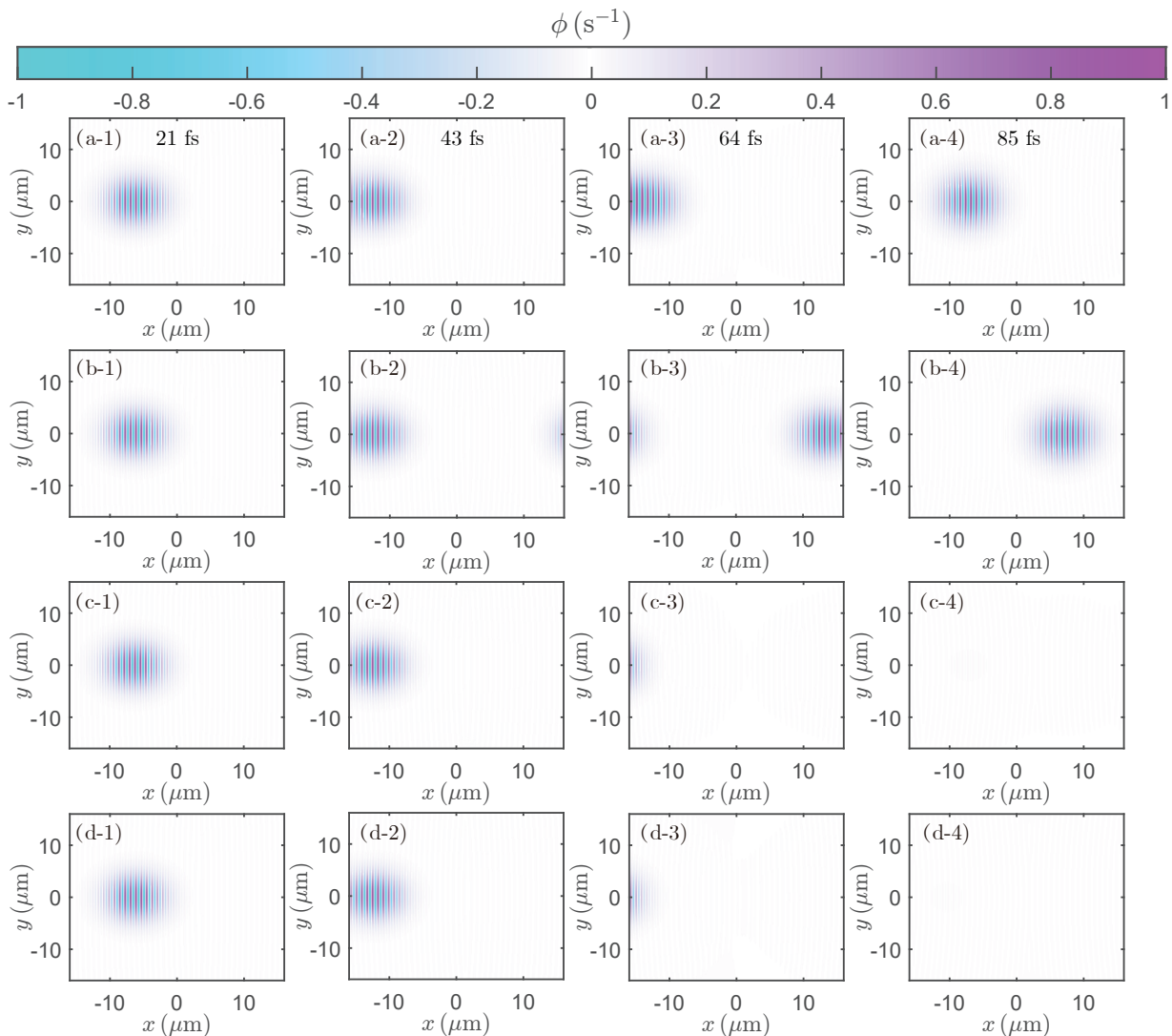


Figure 2. Temporal evolution of the axion field with different boundary conditions. Axion field distribution at different times with different boundary conditions: (a) Reflect, (b) Periodic, (c) Outflow, (d) PML.

FWHM duration is $5T_0 = 5\lambda_0/c$. The magnetic field is set to be 423 T and uniform in space. The laser is propagating in x direction and the simulation window is also moving at the light speed after the laser is injected into it. Moreover, here we assume the axion mass to be 1 meV. As for the coupling constant, there are two primary models for axion-photon coupling: KSVZ (Kim-Shifman-Vainshtein-Zakharov)^{46,47} and DFSZ (Dine-Fischler-Srednicki-Zhitnisky)^{48,49}. Different models would give different coupling constant:

$$m_a = 6.3 \text{ eV} \frac{10^6 \text{ GeV}}{f_a}, \quad (46)$$

$$g_{a\gamma\gamma} = c_\gamma \frac{2\alpha}{\pi f_a}, \quad (47)$$

where $c_\gamma = -0.97$ for KSVZ model and $c_\gamma = 0.36$ for DFSZ model. Here DFSZ axion model is considered. The corresponding coupling constant is $g_{a\gamma\gamma} =$

$2.65 \times 10^{-13} \hbar \text{ GeV}^{-1}$. The KSVZ model would be similar.

Figure 3 shows the result of the axion generation process. The distributions of the laser electric field and axion field at two instants are shown in Fig 3-(a,b). The laser pulse continuously generates axion and the axion field is increasing during the propagation. Meanwhile, we can also see that the laser pulse and the generated axion pulse both gradually defocus due to the finite pulse width.

We also quantitatively compared the conversion probability. The conversion probability in the simulation can be given by the total energy ratio between the axion and

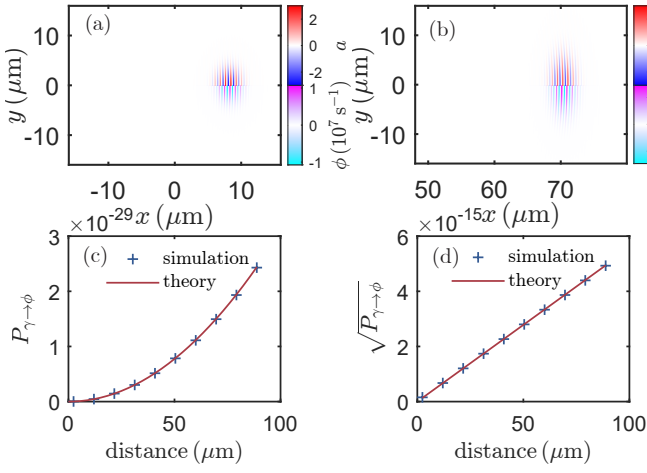


Figure 3. Laser propagation and axion generation in a constant magnetic field. Distribution of normalized laser field $a_y = |eE_y/(m_e\omega_0c)|$ (upper half) and axion field (lower half) after propagating (a) 25 μm and (b) 89 μm . Comparison between the conversion probability from simulation result and theoretical prediction (c) $P_{\gamma\rightarrow\phi}$ and (d) $\sqrt{P_{\gamma\rightarrow\phi}}$ during propagation.

laser pulse in the simulation box,

$$P_{\gamma\rightarrow\phi,\text{sim}} = \frac{H_\phi}{H_\gamma} = \frac{\iint \mathcal{H}_\phi dx dy}{\iint \mathcal{H}_\gamma dx dy}, \quad (48)$$

$$\mathcal{H}_\phi = \frac{\hbar}{2c} \left(\frac{1}{c^2} |\partial_t \phi|^2 + |\nabla \phi|^2 + \frac{m_a^2 c^2}{\hbar^2} \phi^2 \right), \quad (49)$$

$$\mathcal{H}_\gamma = \frac{1}{2} \left(\epsilon_0 E^2 + \frac{1}{\mu_0} B^2 \right). \quad (50)$$

The results are shown in Fig. 3-(c,d). We can see that the conversion probabilities of theory and simulation match each other quite well, and $\sqrt{P_{\gamma\rightarrow\phi}}$ is linear to the propagation distance.

C. Benchmark of Axion Conversion into Photons

In addition, we can also simulate the process of axion conversion into photons. In this case, there is only an axion pulse initially in the simulation box and propagating in the constant magnetic field. The axion pulse is the same as that in Sec. III A, and the magnetic field is the same as that in Sec. III B.

As for this case, the conversion probability in the simulation is also given by the energy ratio,

$$P_{\phi\rightarrow\gamma,\text{sim}} = \frac{H_\gamma}{H_\phi} = \frac{\iint \mathcal{H}_\gamma dx dy}{\iint \mathcal{H}_\phi dx dy}, \quad (51)$$

where the energy density \mathcal{H}_γ of EM fields is given by the first order perturbation \mathbf{E}_1 , \mathbf{B}_1 . The results are also similar to those of photon conversion into axions, as shown in Fig. 4. The laser pulse is continuously generated by

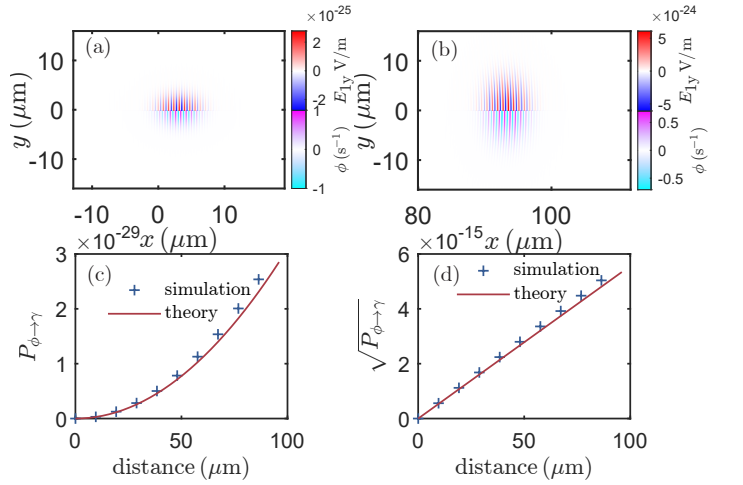


Figure 4. Axion conversion into EM fields. Distribution of perturbed laser field E_y (upper half) and axion field (lower half) after propagating (a) 3 μm and (b) 96 μm . Comparison between the conversion probability (c) $P_{\phi\rightarrow\gamma}$ and (d) $\sqrt{P_{\phi\rightarrow\gamma}}$ during propagation.

the axion pulse, and both two pulses gradually defocus during propagation. The conversion probability obtained from the simulation also matches well with the theory.

D. Benchmark of FPS Method

As described in Sec. II B, we have used the FPS method to solve the problem of floating-point error when there is a significant strength difference between the original and derivative fields. Such a method can also be checked through an extremely weak laser pulse propagating in a magnetized plasma. We consider a laser pulse with $\lambda_0 = 800\text{ nm}$ and a plasma with a density $n_0 = 3 \times 10^{-3} n_c$, where $n_c = \epsilon_0 m_e \omega_0^2 / e^2$ is the critical plasma density. The external magnetic field is set to be $B_c = m_e \omega_p / e$ to magnetize the plasma in z direction, where $\omega_p^2 = n_0 e^2 / (\epsilon_0 m_0)$ is the plasma frequency. The laser pulse is sufficiently weak and the laser magnetic field is $10^{-20} B_c$. The simulation box is $[-20\lambda_0, 20\lambda_0] \times [-50\lambda_0, 50\lambda_0]$, and the space grid number is 12000×100 . Higher spatial accuracy was adopted in x direction, to reduce the impact of numerical dispersion. Such a laser pulse would be overwhelmed by the background magnetic if it is calculated directly. However, its propagation can be correctly calculated though the FPS method.

The refractivity η of a laser in a transversely magnetized plasma is given by⁵⁰:

$$\eta^2 = 1 - \frac{\omega_p^2}{\omega^2} \frac{\omega^2 - \omega_p^2}{\omega^2 - \omega_p^2 - \omega_c^2}, \quad (52)$$

where $\omega_c = eB_c/m_e$ is the electron cyclotron frequency in the magnetic field, and the magnetic field is perpendicular to the laser polarization. The the laser group velocity

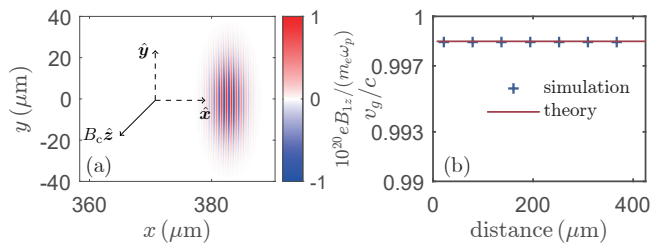


Figure 5. Weak laser propagation in a transversely magnetized plasma. (a) Distribution of the laser magnetic field. (b) Comparison between the laser group velocity from the simulation and theory.

can be given by:

$$v_g = \frac{c\eta}{\eta^2 + \omega^2 \frac{d(\eta^2)}{d(\omega^2)}}. \quad (53)$$

On the other hand, the laser group velocity in the simulation can be given by its centroid trajectory, and it is calculated by:

$$x_{\text{laser}} = \frac{\iint x B_{1z}^2 dx dy}{\iint B_{1z}^2 dx dy}. \quad (54)$$

The results of weak laser propagation are shown in Fig. 5. Figure 5 (a) shows that the sufficiently weak laser pulse can stably propagate in the magnetized plasma, rather than numerically overwhelmed by the background magnetic field. Meanwhile, as Fig. 5 (b) shows, the laser group velocity from the simulation matches well with the theoretical results. In fact, the FPS method can not only solve the EM modulation from the axion fields, but also correctly handling weak lasers in strong background fields.

IV. SUMMARY

In summary, we have proposed and benchmarked a method to model the axion field and the coupling with electromagnetic fields in the PIC code. The axion wave equation and modified Maxwell equations are considered, while the modulation of the axion field to EM fields is treated in first-order perturbation. Different boundary conditions are realized in the code. The conversion processes of axions into photons and photons into axions are checked as benchmarks of the code. The propagation of a weak laser in a strongly magnetized plasma is also checked to illustrate the validity of our FPS method. We hope such a tool can help researchers develop novel axion generation and detection schemes based on laser-plasma interactions and provide a better understanding of the astrophysical processes in which axions participate.

ACKNOWLEDGMENTS

The computations in this paper were run on the π 2.0 cluster supported by the Center for High Performance Computing at Shanghai Jiao Tong University. This work was supported by the National Natural Science Foundation of China (No. 12225505 and No. 11991074).

REFERENCES

- ¹F. Wilczek, “Problem of strong P and T invariance in the presence of instantons,” *Phys. Rev. Lett.* **40**, 279–282 (1978).
- ²S. Weinberg, “A new light boson?” *Phys. Rev. Lett.* **40**, 223–226 (1978).
- ³R. D. Peccei and H. R. Quinn, “CP conservation in the presence of pseudoparticles,” *Phys. Rev. Lett.* **38**, 1440–1443 (1977).
- ⁴R. D. Peccei and H. R. Quinn, “Constraints imposed by CP conservation in the presence of pseudoparticles,” *Phys. Rev. D* **16**, 1791–1797 (1977).
- ⁵J. E. Kim and G. Carosi, “Axions and the strong C P problem,” *Rev. Modern Phys.* **82**, 557–601 (2010).
- ⁶F. Chadha-Day, J. Ellis, and D. J. E. Marsh, “Axion dark matter: What is it and why now?” *Sci. Adv.* **8**, eabj3618 (2022).
- ⁷N. Du, N. Force, R. Khatiwada, E. Lentz, R. Ottens, L. Rosenberg, G. Rybka, G. Carosi, N. Woollett, D. Bowring, A. Chou, A. Sonnenschein, W. Wester, C. Boutan, N. Oblath, R. Bradley, E. Daw, A. Dixit, J. Clarke, S. O’Kelley, N. Crisosto, J. Gleason, S. Jois, P. Sikivie, I. Stern, N. Sullivan, D. Tanner, G. Hilton, and ADMX Collaboration, “Search for invisible axion dark matter with the axion dark matter experiment,” *Phys. Rev. Lett.* **120**, 151301 (2018).
- ⁸T. Braine, R. Cervantes, N. Crisosto, N. Du, S. Kimes, L. Rosenberg, G. Rybka, J. Yang, D. Bowring, A. Chou, R. Khatiwada, A. Sonnenschein, W. Wester, G. Carosi, N. Woollett, L. Duffy, R. Bradley, C. Boutan, M. Jones, B. LaRoque, N. Oblath, M. Taubman, J. Clarke, A. Dove, A. Eddins, S. O’Kelley, S. Nawaz, I. Siddiqi, N. Stevenson, A. Agrawal, A. Dixit, J. Gleason, S. Jois, P. Sikivie, J. Solomon, N. Sullivan, D. Tanner, E. Lentz, E. Daw, J. Buckley, P. Harrington, E. Henriksen, K. Murch, and ADMX Collaboration, “Extended Search for the Invisible Axion with the Axion Dark Matter Experiment,” *Phys. Rev. Lett.* **124**, 101303 (2020).
- ⁹C. Bartram, T. Braine, E. Burns, R. Cervantes, N. Crisosto, N. Du, H. Korandla, G. Leum, P. Mohapatra, T. Nitta, L. Rosenberg, G. Rybka, J. Yang, J. Clarke, I. Siddiqi, A. Agrawal, A. Dixit, M. Awida, A. Chou, M. Hollister, S. Knirck, A. Sonnenschein, W. Wester, J. Gleason, A. Hipp, S. Jois, P. Sikivie, N. Sullivan, D. Tanner, E. Lentz, R. Khatiwada, G. Carosi, N. Robertson, N. Woollett, L. Duffy, C. Boutan, M. Jones, B. LaRoque, N. Oblath, M. Taubman, E. Daw, M. Perry, J. Buckley, C. Gaikwad, J. Hoffman, K. Murch, M. Goryachev, B. McAllister, A. Quiskamp, C. Thomson, M. Tobar, and ADMX Collaboration, “Search for Invisible Axion Dark Matter in the 3.3 - 4.2 μ eV Mass Range,” *Phys. Rev. Lett.* **127**, 261803 (2021).
- ¹⁰CAST Collaboration, “New CAST limit on the axion–photon interaction,” *Nat. Phys.* **13**, 584–590 (2017).
- ¹¹J. W. Foster, Y. Kahn, O. Macias, Z. Sun, R. P. Eatough, V. I. Kondratiev, W. M. Peters, C. Weniger, and B. R. Safdi, “Green Bank and Effelsberg Radio Telescope Searches for Axion Dark Matter Conversion in Neutron Star Magnetospheres,” *Phys. Rev. Lett.* **125**, 171301 (2020).
- ¹²T. D. Edwards, B. J. Kavanagh, L. Visinelli, and C. Weniger, “Transient Radio Signatures from Neutron Star Encounters with QCD Axion Miniclusters,” *Phys. Rev. Lett.* **127**, 131103 (2021).
- ¹³M. Buschmann, R. T. Co, C. Dessert, and B. R. Safdi, “Axion Emission Can Explain a New Hard X-Ray Excess from Nearby Isolated Neutron Stars,” *Phys. Rev. Lett.* **126**, 021102 (2021).

- ¹⁴E. Zavattini, G. Zavattini, G. Ruoso, E. Polacco, E. Milotti, M. Karuza, U. Gastaldi, G. Di Domenico, F. Della Valle, R. Cimino, S. Carusotto, G. Cantatore, and M. Bregant, “Experimental Observation of Optical Rotation Generated in Vacuum by a Magnetic Field,” *Phys. Rev. Lett.* **96**, 110406 (2006).
- ¹⁵R. Battesti, B. Pinto Da Souza, S. Batut, C. Robilliard, G. Bailly, C. Michel, M. Nardone, L. Pinard, O. Portugall, G. Tréneç, J.-M. Mackowski, G. L. Rikken, J. Vigué, and C. Rizzo, “The BMV experiment: a novel apparatus to study the propagation of light in a transverse magnetic field,” *Eur. Phys. J. D* **46**, 323–333 (2008).
- ¹⁶R. Cameron, G. Cantatore, A. Melissinos, G. Ruoso, Y. Semertzidis, H. Halama, D. Lazarus, A. Prodell, F. Nezzrick, C. Rizzo, and E. Zavattini, “Search for nearly massless, weakly coupled particles by optical techniques,” *Phys. Rev. D* **47**, 3707–3725 (1993).
- ¹⁷S.-J. Chen, H.-H. Mei, and W.-T. Ni, “Q & a experiment to search for vacuum dichroism, pseudoscalar–photon interaction and millicharged fermions,” *Mod. Phys. Lett. A* **22**, 2815–2831 (2007).
- ¹⁸K. Ehret, M. Frede, S. Ghazaryan, M. Hildebrandt, E.-A. Knabbe, D. Kracht, A. Lindner, J. List, T. Meier, N. Meyer, D. Notz, J. Redondo, A. Ringwald, G. Wiedemann, and B. Willke, “New ALPS results on hidden-sector lightweights,” *Phys. Lett. B* **689**, 149–155 (2010).
- ¹⁹A. S. Chou, W. Wester, A. Baumbaugh, H. R. Gustafson, Y. Irizarry-Valle, P. O. Mazur, J. H. Steffen, R. Tomlin, X. Yang, and J. Yoo, “Search for axionlike particles using a variable-baseline photon-regeneration technique,” *Phys. Rev. Lett.* **100**, 80402 (2008).
- ²⁰A. Afanasev, O. K. Baker, K. B. Beard, G. Biallas, J. Boyce, M. Minarni, R. Ramdon, M. Shinn, and P. Slocum, “Experimental Limit on Optical-Photon Coupling to Light Neutral Scalar Bosons,” *Phys. Rev. Lett.* **101**, 120401 (2008).
- ²¹P. Pugnât, L. Duvillaret, R. Jost, G. Vitrant, D. Romanini, A. Siemko, R. Ballou, B. Barbara, M. Finger, M. Finger, J. Hošek, M. Král, K. A. Meissner, M. Šulc, and J. Zicha, “Results from the OSQAR photon-regeneration experiment: No light shining through a wall,” *Phys. Rev. D* **78**, 92003 (2008).
- ²²C. Robilliard, R. Battesti, M. Fouché, J. Mauchain, A.-M. Sautivet, F. Amiranoff, and C. Rizzo, “No ‘Light Shining through a Wall’: Results from a Photoregeneration Experiment,” *Phys. Rev. Lett.* **99**, 190403 (2007).
- ²³S. Li, M. Wu, A. Abdurkerim, Z. Bo, W. Chen, X. Chen, Y. Chen, C. Cheng, Z. Cheng, X. Cui, Y. Fan, D. Fang, C. Fu, M. Fu, L. Geng, K. Giboni, L. Gu, X. Guo, C. Han, K. Han, C. He, J. He, D. Huang, Y. Huang, Z. Huang, R. Hou, X. Ji, Y. Ju, C. Li, J. Li, M. Li, S. Li, Q. Lin, J. Liu, X. Lu, L. Luo, Y. Luo, W. Ma, Y. Ma, Y. Mao, Y. Meng, X. Ning, N. Qi, Z. Qian, X. Ren, N. Shaheed, C. Shang, X. Shang, G. Shen, L. Si, W. Sun, A. Tan, Y. Tao, A. Wang, M. Wang, Q. Wang, S. Wang, S. Wang, W. Wang, X. Wang, Z. Wang, Y. Wei, W. Wu, J. Xia, M. Xiao, X. Xiao, P. Xie, B. Yan, X. Yan, J. Yang, Y. Yang, Y. Yao, Z. You, C. Yu, J. Yuan, Y. Yuan, Z. Yuan, X. Zeng, D. Zhang, M. Zhang, P. Zhang, S. Zhang, S. Zhang, T. Zhang, Y. Zhang, Y. Zhang, Y. Zhang, L. Zhao, Q. Zheng, J. Zhou, N. Zhou, X. Zhou, Y. Zhou, Y. Zhou, and PandaX Collaboration, “Search for light dark matter with ionization signals in the PandaX-4T experiment,” *Phys. Rev. Lett.* **130**, 261001 (2023).
- ²⁴V. Dinu, T. Heinzl, A. Ilderton, M. Marklund, and G. Torgrimsson, “Vacuum refractive indices and helicity flip in strong-field QED,” *Phys. Rev. D* **89**, 125003 (2014).
- ²⁵B. Shen, Z. Bu, J. Xu, T. Xu, L. Ji, R. Li, and Z. Xu, “Exploring vacuum birefringence based on a 100 PW laser and an x-ray free electron laser beam,” *Plasma Phys. Controlled Fusion* **60**, 44002 (2018).
- ²⁶Y.-N. Dai, K. Z. Hatsagortsyan, C. H. Keitel, and Y.-Y. Chen, “Fermionic signal of vacuum polarization in strong laser fields,” (2024), arXiv:2401.11168 [hep-th].
- ²⁷H. Terças, J. Rodrigues, and J. Mendonça, “Axion-Plasmon Polaritons in Strongly Magnetized Plasmas,” *Phys. Rev. Lett.* **120**, 181803 (2018).
- ²⁸J. T. Mendonça, H. Terças, and J. D. Rodrigues, “Axion excitation by intense laser fields in a plasma,” *Phys. Scr.* **95**, 045601 (2020).
- ²⁹J. Mendonça, J. Rodrigues, and H. Terças, “Axion production in unstable magnetized plasmas,” *Phys. Rev. D* **101**, 051701 (2020).
- ³⁰S. Huang, B. Shen, Z. Bu, X. Zhang, L. Ji, and S. Zhai, “Axion-like particle generation in laser-plasma interaction,” *Phys. Scr.* **97**, 105303 (2022).
- ³¹S. P. D. Mangles, C. D. Murphy, Z. Najmudin, A. G. R. Thomas, J. L. Collier, A. E. Dangor, E. J. Divall, P. S. Foster, J. G. Gallacher, C. J. Hooker, D. A. Jaroszynski, A. J. Langley, W. B. Mori, P. A. Norreys, F. S. Tsung, R. Viskup, B. R. Walton, and K. Krushelnick, “Monoenergetic beams of relativistic electrons from intense laser–plasma interactions,” *Nature* **431**, 535–538 (2004).
- ³²C. G. R. Geddes, C. Toth, J. Van Tilborg, E. Esarey, C. B. Schroeder, D. Bruhwiler, C. Nieter, J. Cary, and W. P. Leemans, “High-quality electron beams from a laser wakefield accelerator using plasma-channel guiding,” *Nature* **431**, 538–541 (2004).
- ³³J. Faure, Y. Glinec, A. Pukhov, S. Kiselev, S. Gordienko, E. Lefebvre, J.-P. Rousseau, F. Burgy, and V. Malka, “A laser–plasma accelerator producing monoenergetic electron beams,” *Nature* **431**, 541–544 (2004).
- ³⁴X. An, M. Chen, S. Weng, Z. Sheng, and J. Zhang, “Bragg scattering induced laser deflection and electron injection in x-ray laser driven wakefield acceleration in crystals,” *Phys. Rev. Research* **4**, L042034 (2022).
- ³⁵A. Gonoskov, S. Bastrakov, E. Efimenko, A. Ilderton, M. Marklund, I. Meyerov, A. Muraviev, A. Sergeev, I. Surmin, and E. Wallin, “Extended particle-in-cell schemes for physics in ultrastrong laser fields: Review and developments,” *Phys. Rev. E* **92**, 023305 (2015).
- ³⁶H.-H. Song, W.-M. Wang, and Y.-T. Li, “Dense Polarized Positrons from Laser-Irradiated Foil Targets in the QED Regime,” *Phys. Rev. Lett.* **129**, 035001 (2022).
- ³⁷T. D. Arber, K. Bennett, C. S. Brady, A. Lawrence-Douglas, M. G. Ramsay, N. J. Sircombe, P. Gillies, R. G. Evans, H. Schmitz, A. R. Bell, and C. P. Ridgers, “Contemporary particle-in-cell approach to laser-plasma modelling,” *Plasma Phys. Control. Fusion* **57**, 113001 (2015).
- ³⁸L. Visinelli, “Axion-electromagnetic waves,” *Modern Phys. Lett. A* **28**, 1350162 (2013).
- ³⁹C. P. Ridgers, C. S. Brady, R. Ducloux, J. G. Kirk, K. Bennett, T. D. Arber, A. P. L. Robinson, and A. R. Bell, “Dense electron-positron plasmas and ultraintense γ rays from laser-irradiated solids,” *Phys. Rev. Lett.* **108**, 165006 (2012).
- ⁴⁰P.-J. Charpin, K. Ardaneh, B. Morel, R. Giust, and F. Courvoisier, “Simulation of laser-induced ionization in wide bandgap solid dielectrics with a particle-in-cell code,” *Opt. Express* **32**, 10175–10189 (2024).
- ⁴¹J. Vyskočil, O. Klimo, and S. Weber, “Simulations of bremsstrahlung emission in ultra-intense laser interactions with foil targets,” *Plasma Phys. Controlled Fusion* **60**, 54013 (2018).
- ⁴²J.-P. Berenger, “A perfectly matched layer for the absorption of electromagnetic waves,” *J. Comput. Phys.* **114**, 185–200 (1994).
- ⁴³J. A. Roden and S. D. Gedney, “Convolution PML (CPML): An efficient FDTD implementation of the CFS–PML for arbitrary media,” *Microw. Opt. Technol. Lett.* **27**, 334–339 (2000).
- ⁴⁴A. F. Oskooi, L. Zhang, Y. Avniel, and S. G. Johnson, “The failure of perfectly matched layers, and towards their redemption by adiabatic absorbers,” *Opt. Express* **16**, 11376 (2008).
- ⁴⁵P. Arias, J. Jaeckel, J. Redondo, and A. Ringwald, “Optimizing light-shining-through-a-wall experiments for axion and other weakly interacting slim particle searches,” *Phys. Rev. D* **82**, 115018 (2010).
- ⁴⁶J. E. Kim, “Weak-interaction singlet and strong CP invariance,” *Phys. Rev. Lett.* **43**, 103–107 (1979).

⁴⁷M. Shifman, A. Vainshtein, and V. Zakharov, “Can confinement ensure natural CP invariance of strong interactions?” Nucl. Phys. B **166**, 493–506 (1980).

⁴⁸A. R. Zhitnitskij, “On possible suppression of the axion-hadron interactions,” Sov. J. Nucl. Phys. **31**, 260 (1980).

⁴⁹M. Dine, W. Fischler, and M. Srednicki, “A simple solution to the strong CP problem with a harmless axion,” Phys. Lett. B **104**, 199–202 (1981).

⁵⁰F. F. Chen, *Introduction to plasma physics and controlled fusion* (Springer International Publishing, Cham, 2016).